Inorganic Chemistry

Article

pubs.acs.org/IC

Pressure-Induced Transformations in $PrVO_4$ and $SmVO_4$ and Isolation of High-Pressure Metastable Phases

Daniel Errandonea,*[,†] S. Nagabhusan Achary,[‡] Julio Pellicer-Porres,[†] and Avesh K. Tyagi[‡]

[†]Departamento de Física Aplicada-ICMUV, Universidad de Valencia, MALTA Consolider Team, Edificio de Investigación, C/Dr. Moliner 50, 46100 Burjassot, Valencia, Spain

[‡]Chemistry Division, Bhabha Atomic Research Centre, Trombay, Mumbai 400085, India

ABSTRACT: Zircon-type $PrVO_4$ and $SmVO_4$ have been studied by high-pressure Raman spectroscopy up to 17 GPa. The occurrence of phase transitions has been detected when compression exceeds 6 GPa. The transformations are not reversible. Raman spectra of the high-pressure phases show similarities with those expected for a monazite-type phase in $PrVO_4$ and a scheelite-type phase in $SmVO_4$.The high-pressure phases have been also synthesized using a large-volume press and recovered at ambient conditions. X-ray diffraction measurements of the metastable products recovered after decompression confirms the monazite ($PrVO_4$) and scheelite ($SmVO_4$) structures of the high-pressure phases. Based upon optical properties of the reported new polymorphs, novel applications for rare-earth vanadates are proposed, including photocatalytic hydrogen production.

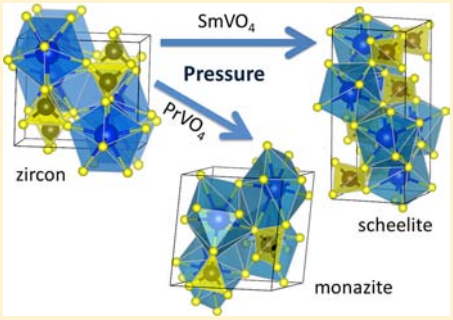

1. INTRODUCTION

Rare-earth orthovanadates have a number of important applications;[1] e.g., in cathodoluminescence and lithium ion batteries, as well as thermophosphors, scintillators, photocatalysis materials, and laser-host materials. With the exception of $LaVO_4$, they crystallize in the tetragonal zircon-type structure (space group: $I4_1/amd$, $Z = 4$).[2] Under moderate compression, these compounds undergo transformations to denser phases.[3−5] In particular, compounds with small rare-earth cations transform to the tetragonal scheelite-type structure (space group: $I4_1/a$, $Z = 4$) while those with large cations transform to the monoclinic monazite-type structure (space group: $P2_1/n$, $Z = 4$). Both phase transformations have attracted much attention[6−9] because they are interesting for technological applications, geophysics, and geochemistry. Among the zircon-type rare-earth orthovanadates, praseodymium vanadate ($PrVO_4$) and samarium vanadate ($SmVO_4$) are the less studied systems under pressure. To shed more light on the understanding of the structural properties of zircon-type oxides and in particular the pressure-induced phase transitions of rare-earth vanadates, we have studied the high-pressure behavior of both $PrVO_4$ and $SmVO_4$ up to 17 GPa. The Raman-active modes and their pressure behavior of the low- and high-pressure (HP) phases are determined. Further, the high-pressure phases of both materials have been prepared, and their crystal structures are reported. A potential pressure-induced band gap collapse in zircon-type rare-earth vanadates is also discussed.

2. EXPERIMENTAL METHODS

$PrVO_4$ and $SmVO_4$ were studied in situ under compression by Raman spectroscopy. Experiments were performed using a diamond-anvil cell and a 16:3:1 methanol−ethanol−water mixture as pressure-transmitting medium.[10] Pressure was determined using the ruby scale,[11] and Raman spectra were collected in the backscattering geometry using a 488 nm Ar laser and a Jobin−Yvon spectrometer in combination with a thermoelectric-cooled multichannel CCD detector with spectral resolution below 2 cm^{-1}. A laser power of less than 10 mW before the DAC was used to avoid sample heating. Three experimental runs were carried out for each compound with similar results.

Polycrystalline $PrVO_4$ and $SmVO_4$ used in the experiments were prepared by solid-state reaction of appropriate amounts of 99% purity predried Pr_6O_{11} or Sm_2O_3 and V_2O_5 in a platinum crucible. The homogeneous mixtures of the samples were heated at 600 °C for 24 h and then reground and pelleted. The pellets were heated at 900 °C for 24 h. Finally, the products were further heated at 1100 °C for another 12 h. The obtained samples were characterized at ambient conditions by X-ray diffraction (XRD) data recorded on a Panalytical X-pert Pro diffractometer using Cu K_α radiation ($\lambda = 1.5418$ Å). A single phase with the zircon-type structure was confirmed for $PrVO_4$ and $SmVO_4$. The obtained unit-cell parameters agree within 0.1% with the literature;[12,13] $a = 7.3618(2)$ Å and $c = 6.4634(3)$ Å for $PrVO_4$ and $a = 7.2618(2)$ Å and $c = 6.3837(3)$ Å for $SmVO_4$.

The HP phases of $PrVO_4$ and $SmVO_4$ have been also synthesized at a pressure of 12 GPa and room temperature starting from zircon-structured compounds. Pressure was applied for 24 h using a 150 ton hydraulic press equipped with steel-belted Bridgman-type opposed tungsten-carbide anvils.[14] Pressure was released rapidly at ∼3 GPa/min to quench the HP phases of both vanadates. The samples were contained in a thermal-treated pyrophyllite chamber and inserted inside it. The pressure-transmitting medium was hexagonal boron nitride. The sample pressure was determined by the calibration of the load applied to the anvils against HP resistivity transitions in calibrants.[15] The recovered metastable products were analyzed by XRD to determine their crystal structures.

Received: February 13, 2013
Published: April 19, 2013

dx.doi.org/10.1021/ic400376g | Inorg. Chem. 2013, 52, 5464−5469

3. RESULTS AND DISCUSSION

The zircon structure ($I4_1/amd$, point group D_{4h}) has two formula units per primitive cell. According to group-theory analysis, it has 12 Raman-active modes at the center of the Brilllouin zone (BZ) with symmetries $\Gamma = 2A_{1g} + 4B_{1g} + B_{2g} + 5E_g$.[16] These modes can be classified into internal and external modes of the VO_4 units.

Figures 1 and 2 show representative Raman spectra of $PrVO_4$ and $SmVO_4$. In both compounds, at low pressure we have

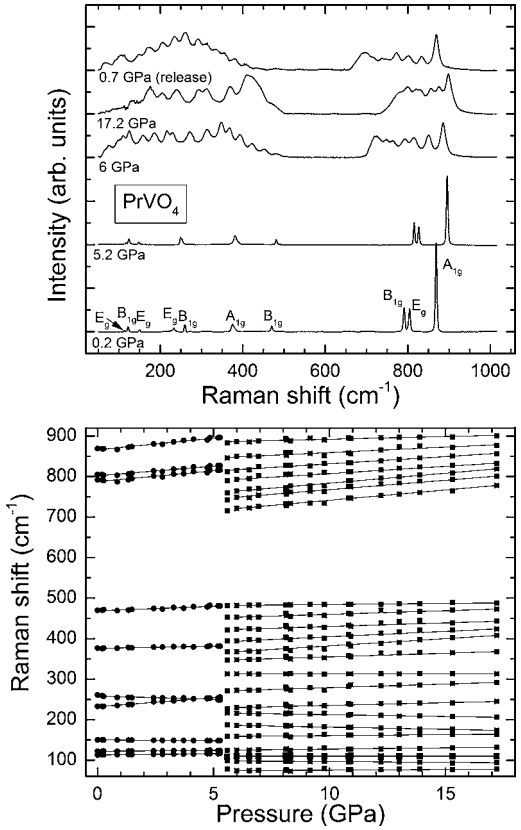

Figure 1. (Top) Selection of high-pressure Raman spectra measured in $PrVO_4$. (Bottom) Pressure evolution of the Raman modes of the different phases. Circles: low-pressure phase. Squares: high-pressure phase.

observed 10 out of 12 expected Raman peaks. All the Raman modes observed can be divided into two broad frequency regions, the low-frequency region from 100 to 480 cm^{-1} and the high-frequency region from 790 to 880 cm^{-1}, with a frequency gap between them. The symmetry assignment for the Raman modes has been performed in accordance with the literature.[16] Raman-mode frequencies (ω) are summarized in Table 1. They agree well with the frequencies reported by Santos et al.[16]As can be seen from Figures 1 and 2, the Raman spectra of the two studied vanadates are dominated by the intense high-frequency modes, which are associated with internal stretching modes.[16]Regarding the two undetected Raman modes, they are usually not observed in zircon-type oxides, their absence being probably due to their weak Raman scattering cross-section.[16,17]

Upon compression, the Raman spectra of both compounds remain like that expected for the zircon phase up to about 6 GPa. From Raman spectra collected at different pressures, we obtained the pressure evolution of the different Raman modes.

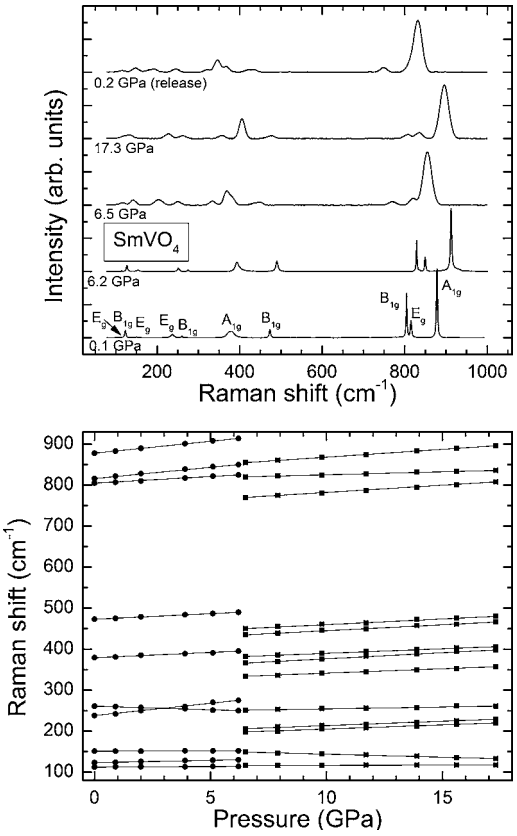

Figure 2. (Top) Selection of high-pressure Raman spectra measured in $SmVO_4$. (Bottom) Pressure evolution of the Raman modes of the different phases. Circles: low-pressure phase. Squares: high-pressure phase.

These results are summarized in Figures 1 and 2 for $PrVO_4$ and $SmVO_4$, respectively. There it can be seen that as a first approximation they depend linearly upon pressure. The obtained pressure coefficients for each mode ($d\omega/dP$) are also given in Table 1. In $PrVO_4$, all the Raman modes of the zircon phase exhibit positive pressure coefficients except for a low-frequency E_g mode and a low-frequency B_{2g} mode. In $SmVO_4$ only one of these modes shows such a soft-mode behavior (see Table 1). Some modes merge or cross upon compression due to their different pressure evolution (see Figures 1 and 2). The modes that change more under compression (larger $d\omega/dP$) are the internal high-frequency modes and the low-frequency E_g mode with frequency near 235 cm^{-1}. This mode is a rotational mode. Due to its large pressure coefficient, upon compression there is a crossover of this E_g mode with a B_{1g} mode, which has a higher frequency at ambient pressure (261 cm^{-1}). A similar high-pressure behavior has been observed in Raman modes of $ScVO_4$,[18] $LuVO_4$,[19] $CeVO_4$,[20] $YbVO_4$,[21] $DyVO_4$,[22] $TbVO_4$,[22] $SmVO_4$,[23] and $GdVO_4$.[24] The mode softening observed is typical of zircon-type vanadates and phosphates and, despite the mode not reaching zero frequency, has been associated with a mechanical instability of the zircon phase, leading to phase transitions.[25]

In Figures 1 and 2 it can be seen that remarkable changes take place in the Raman spectra at 6 GPa in $PrVO_4$ and at 6.5 GPa in $SmVO_4$. The changes are indicative of the onset of a phase transition. In the case of $PrVO_4$, the Raman spectra of the new HP phase are similar to those expected from a monazite-structured phase.[26,27] For $SmVO_4$, the Raman spectra of the

dx.doi.org/10.1021/ic400376g | Inorg. Chem. 2013, 52, 5464−5469

Table 1. Phonon Frequencies ω (in cm^{-1}) and Pressure Coefficients $d\omega/dP$ (in cm^{-1}/GPa) for Zircon-Type $PrVO_4$ and $SmVO_4$ at Ambient Pressure, for Monazite-Type $PrVO_4$ at 6 GPa, and for Scheelite-Type $SmVO_4$ at 6.5 GPa

$PrVO_4$						$SmVO_4$					
zircon			monazite			zircon			scheelite		
mode	ω	$d\omega/dP$	mode	ω	$d\omega/dP$	mode	ω	$d\omega/dP$	mode	ω	$d\omega/dP$
E_g	113	0.66	lattice	74	0.64	E_g	112	0.32	E_g	116	0.09
B_{1g}	122	0.44	lattice	98	−0.36	B_{1g}	123	1.1	B_g	149	−1.4
E_g	150	−0.37	lattice	110	0.03	E_g	151	0.16	B_g	198	2.0
E_g	233	4.3	lattice	124	0.62	E_g	238	5.9	E_g	206	2.1
B_{1g}	261	−1.6	lattice	159	0.44	B_{1g}	261	−1.8	A_g	251	0.89
B_{2g}	–	–	lattice	186	−1.1	B_{2g}	–	–	E_g	334	2.1
A_{1g}	377	1.1	lattice	216	−0.89	A_{1g}	379	2.6	A_g	366	2.9
E_g	–	–	lattice	230	1.3	E_g	–	–	B_g	382	2.1
B_{1g}	470	2.0	bending	272	1.8	B_{1g}	473	2.7	B_g	435	1.9
B_{1g}	792	4.6	bending	313	0.02	B_{1g}	805	3.2	E_g	450	2.1
E_g	805	4.2	bending	348	1.8	E_g	816	5.4	E_g	770	3.4
A_{1g}	869	5.1	bending	368	3.6	A_{1g}	878	5.8	B_g	820	1.5
			bending	394	3.2				A_g	855	3.7
			bending	423	1.8						
			bending	453	1.8						
			bending	482	0.54						
			stretching	721	5.0						
			stretching	749	4.6						
			stretching	764	4.9						
			stretching	793	3.6						
			stretching	815	3.7						
			stretching	850	2.3						
			stretching	886	1.25						

new HP phase resemble those of a scheelite-structured phase.[28,29] Confirmation of these structures was obtained from XRD measurements on synthesized samples at 12 GPa. The structural refinements will be discussed after commenting on Raman measurements. No additional structural changes are detected upon further compression up to the maximum pressure covered by the Raman experiments (~17 GPa). Upon pressure release, the Raman spectra of the recovered phases are qualitatively similar to those of the HP phases, indicating that the transitions are not reversible.

Monazite-structured compounds (space group: $P2_1/n$, point group: C_{2h}^5) have 36 Raman-active modes at the Γ point: $\Gamma = 18A_g + 18B_g$.[26] However, usually in monazite oxides, no more than 26 modes have been detected.[26,27] In the case of monazite-type $PrVO_4$ we found 23 Raman-active phonons, which are summarized in Table 1. Their frequencies were determined by means of a multipeak fitting using Voigt line shapes after background subtraction. Mode identification as A_g and B_g is not performed for monazite $PrVO_4$ because it requires polarized Raman experiments, which could not be performed because of the powder samples used in the experiments and the lack of polarization of the diamond anvils at high pressure. In Table 1, it can be seen that the Raman spectrum of monazite-type $PrVO_4$ has seven high-frequency modes. They are most likely due to stretching motions within the vanadate ion[30] as indicated in Table 1. The most intense mode is the one at 886 cm^{-1} at 6 GPa. In addition, the Raman spectrum shows eight modes in the 272−482 cm^{-1} wavenumber region, which probably corresponds to bending vibrations of the VO_4 units.[30] Finally, we detected eight vibrations in the low wavenumber region of the spectrum (ω < 230 cm^{-1}), which might originate from external lattice vibrations.[30] From the analysis of Raman spectra collected from 6 to 17.2 GPa, we obtained the pressure dependence of the modes assigned to the HP phase. The results are shown in Figure 1, and the pressure coefficients are summarized in Table 1. The most distinctive feature of the pressure evolution of Raman modes is that pressure tends to have a larger influence in high-frequency modes than in low-frequency modes. It is also noticeable that there are three modes with negative pressure coefficients (soft modes); see Table 1. There is also a tendency to mode merge as pressure increases because of different pressure behaviors of different modes. This can be clearly seen in Figure 1. Most of these described features resemble those observed for monazite-type $CeVO_4$.[20]

Scheelite-type $SmVO_4$ (space group: $I4_1/a$, point group: C_{4h}^6) has 13 zone-center Raman-active modes: $\Gamma = 3A_g + 5B_g + 5E_g$.[28] These vibrations have been classified either as internal, when the VO_4 center of mass does not move, or as external, when they imply movement of VO_4 tetrahedra as rigid units.[29] In the case of scheelite-type $SmVO_4$, after a multipeak fitting, we found all Raman-active phonons, which are summarized in Table 1. The phonon assignment was made following the assignment made in related vanadates.[18−20] The highest frequency mode is the most intense one, which is a distinctive feature of the scheelite structure. The five modes with frequencies larger than 366 cm^{-1} can be assigned to internal vibrations and the five modes with frequencies smaller than 334 cm^{-1} to external vibrations.[18−20] There is only one discrepancy with a recent work[1] where 13 modes of scheelite $SmVO_4$ are reported at ambient pressure. The authors have reported a lowest phonon frequency mode at 148 cm^{-1}, while the lowest phonon mode observed for $SmVO_4$ in this study and in other related compounds[18−20] is near 110 cm^{-1}. In addition, in ref 1 there is a phonon reported near 180 cm^{-1} not found in this work and in the Raman experiments of Patel et al.[23] We think

dx.doi.org/10.1021/ic400376g | Inorg. Chem. 2013, 52, 5464−5469

these discrepancies might be due to an incorrect assignment of modes in ref 1. However, the Raman spectral information provided in Supporting Information of ref 1 agrees with the findings of the present study. Regarding the HP evolution of Raman modes, results are similar to those reported by Patel et al.,[23] who report a phase transition at 6.8 GPa. The Raman spectra of the HP phase published by these authors resemble very much the spectra reported here. The pressure dependence of the Raman modes is shown in Figure 2, and the pressure coefficients are summarized in Table 1. As typical in scheelites, the internal modes have larger pressure coefficients than the external ones, and one of these external modes is a soft mode (see Table 1). Another feature to mention is that no phonon crossover occurs in the pressure range covered by experiments. Regarding the high-frequency mode of the scheelite phase, this mode has been shown to have a frequency that does not depend on the rare-earth cation; i.e., it is an ideal internal mode of the VO_4 tetrahedra. Its frequency is usually 823−830 cm^{-1}.[18] In our case, at 0.2 GPa after decompression we obtained a frequency of 830 cm^{-1}, which is in good agreement with the conclusion extracted by Panchal et al.[18] This frequency is also similar to the ambient pressure frequency (832 cm^{-1}) reported by Huang et al.[1] Note that the mode under discussion is also the one with the highest pressure coefficient.

To unequivocally conclude that the HP phase observed in $PrVO_4$ ($SmVO_4$) has a structure isomorphic to monazite (scheelite), we performed XRD measurements in a sample quenched in a large-volume press cell from 12 GPa. Because the observed transitions are not reversible, the recovered samples retain the crystal structure of the HP phase. Pressures exceeding 5−6 GPa of the transition pressure were needed to recover a sample completely transformed to the HP phase at room temperature. Further, from the Rietveld refinements of the measured patterns, we confirmed the HP structure of $PrVO_4$ and $SmVO_4$ as the monazite and scheelite, respectively.

The refinements of the XRD pattern of the scheelite structure of $SmVO_4$ were carried out using the positions of known structural details of scheelite-type structures.[31] The unit-cell parameters are obtained by indexing the observed reflections. The background of the diffraction data was modeled by a fifth order polynomial function, and peak profile was generated by a pseudo-Voigt profile function. After a proper profile matching, the oxygen positions and isotropic displacement (B) parameters of all atoms were refined. In a similar manner, the XRD pattern of monazite-type $PrVO_4$ was refined using as initial values the observed unit-cell parameters and structural parameters of monazite type $LaVO_4$.[32] In monazite-type structure all the atoms are located in general positions ($4e$) of space group $P2_1/n$ with occupancy 1. The isotropic thermal parameters of all atoms are fixed (B = 0.5 $Å^2$) in the starting model structure, but they were relaxed for the final structural refinement. The background was fitted by linear interpolation of 45 selected points. The peak profile and asymmetry parameters were refined along with the unit-cell parameters. Subsequently, the position coordinates of cations and anions were refined along with isotropic thermal parameters. An appreciable good profile match and residuals are obtained in both cases. The refined structural detail and residuals of refinements are given in Table 2. The observed and calculated XRD patterns for HP phases of $PrVO_4$ and $SmVO_4$ are shown in Figure 3.

The refined structural parameters of monazite-type $PrVO_4$ resemble very closely those of monazite-type $LaVO_4$ and $CeVO_4$.[4,20,32] The obtained unit-cell parameters of scheelite-type $SmVO_4$ are very similar to those of scheelite-type $SmVO_4$ reported by Huang et al.[1] The structural parameters are closely similar to those of the scheelite-type $ErVO_4$.[33] The zircon−monazite transition produces a volume collapse in $PrVO_4$. At ambient pressure, the volume of monazite is 8.5% smaller than that of zircon. Likewise, the zircon−scheelite transition induces a volume collapse in $SmVO_4$. At ambient pressure, the volume of scheelite is about 11.9% smaller than that of zircon. For both structures, the typical interatomic distances are shown in Table 3. In scheelite structure, Sm has eight coordination polyhedra and V has tetrahedral coordination. In monazite, Pr has nine

Table 2. Refined Crystallographic Parameters for Monazite-Type $PrVO_4$ and Scheelite-Type $SmVO_4$ (Ambient Conditions)

atoms	Wyckoff position	x	y	z	B (Å)^2
		Monazite-Type $PrVO_4$[a]			
Pr	4e	0.2833(2)	0.1585(2)	0.1017(2)	0.86(3)
V	4e	0.3069(2)	0.1634(2)	0.6132(2)	0.69(9)
O_1	4e	0.2510(15)	−0.0010(5)	0.4237(6)	2.0(4)
O_2	4e	0.3904(6)	0.3449(4)	0.4959(6)	3.4(3)
O_3	4e	0.4863(7)	0.1122(9)	0.8266(4)	4.7(4)
O_4	4e	0.1230(7)	0.2212(16)	0.7184(6)	2.0(4)
		Scheelite-Type $SmVO_4$[b]			
Sm	4b	0	0.25	0.625	0.9(1)
V	4a	0	0.25	0.125	1.0(2)
O	16f	0.2507(13)	0.1101(13)	0.0464(5)	3.2(4)

[a] $PrVO_4$ (Monoclinic, $P2_1/n$): a = 6.9550(1) Å, b = 7.1652(1) Å, c = 6.6851(1) Å, β = 105.224(1)°; V = 321.46(1) $Å^3$. R_p = 9.63, R_{wp} = 13.9, R_{exp} = 5.92, R_B = 7.10. [b] $SmVO_4$ (Tetragonal, $I4_1/a$): a = 5.1090(1) Å, c = 11.4113(3) Å, V = 297.86(1) $Å^3$. R_p = 9.77, R_{wp} = 12.6, R_{exp} = 7.27, R_B = 4.03.

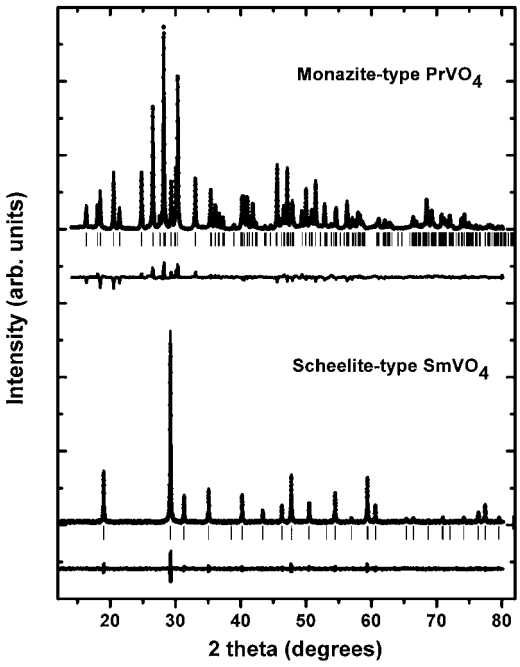

Figure 3. Background-subtracted XRD patterns obtained from recovered monazite-type $PrVO_4$ and scheelite-type $SmVO_4$. Experimental data (dots) and calculated diffraction patterns (solid lines) are shown together with the residuals of the refinement. The ticks indicate the position of the calculated reflections.

dx.doi.org/10.1021/ic400376g | Inorg. Chem. 2013, 52, 5464−5469

Table 3. Typical Interatomic Distances in Monazite-Type $PrVO_4$ and Scheelite-Type $SmVO_4$ (Ambient Conditions)

$PrVO_4$ (monazite)		$SmVO_4$ (scheelite)	
Pr−O_1 × 1	2.499(5) Å	Sm−O × 4	2.441(2) Å
Pr−O_1 × 1	2.453(4) Å	Sm−O × 4	2.411(6) Å
Pr−O_2 × 1	2.554(3) Å	⟨Sm−O⟩	2.426 Å
Pr−O_2 × 1	2.637(4) Å	V−O × 4	1.719(6) Å
Pr−O_2 × 1	2. 873(4) Å		
Pr−O_3 × 1	2.617(5) Å		
Pr−O_3 × 1	2.482(6) Å		
Pr−O_4 × 1	2.5526(2) Å		
Pr−O_4 × 1	2.4425(2) Å		
⟨Pr−O⟩	2.568 Å		
V−O_1 × 1	1.699(4) Å		
V−O_2 × 1	1.698(4) Å		
V−O_3 × 1	1.671(4) Å		
V−O_4 × 1	1.666(5) Å		
⟨V−O⟩	1.683 Å		

coordination polyhedra and V has tetrahedral coordination. In scheelite $SmVO_4$, the average Sm−O bond distance (2.426 Å) and the V−O distance (1.719 Å) are very similar to those in the zircon polymorph, 2.426 Å and 1.710 Å, respectively.[13] This fact indicates that the transformation from zircon to scheelite basically involves a reorientation of VO_4 tetrahedra and SmO_8 dodecahedra. Additionally, the difference between the large and short Sm−O bonds is reduced from 0.115 Å in zircon to 0.026 Å in scheelite; i.e., the SmO_8 dodecahedra become more regular in the HP polymorph. When bond distances in zircon and monazite $PrVO_4$ are compared, it can be concluded that in monazite the VO_4 tetrahedra is highly distorted with four different bond distances. In addition, the average distance V−O distance of monazite $PrVO_4$ (1.683 Å) is 1.5% smaller than the V−O distance in zircon $PrVO_4$ (1.712 Å).[12] On the other hand, the average Pr−O bond distance is larger in monazite (2.568 Å) than in zircon (2.467 Å).[12] This is a consequence of the coordination increase of the Pr atom (from eight to nine) that occurs associated to the phase transition.

The transition mechanisms involved in the two observed phase transitions have been already discussed in the literature.[34−36] The zircon−monazite transition is a first-order transition in which the reduction in the volume and change in polyhedron coordination of Pr are accomplished by breaking a Pr−O bond in zircon and adding two new Pr−O bonds, which makes monazite much more compact than zircon. Basically, these rearrangements produce the addition of a bond in the equatorial plane of the Pr polyhedron, which is added in the void space between the polyhedra of zircon. These atomic changes occur together with a shift of the (001) planes and a slight rotation of the VO_4 tetrahedra, favoring the observed structural changes. Also, the zircon−scheelite transition is reconstructive. This fact explains why the scheelite and monazite phases are metastable at ambient pressure and why the studied vanadates do not revert to the zircon phase after release of pressure due to kinetically higher stability of scheelite and monazite. In particular, during the zircon−scheelite transition the lattice undergoes a homogeneous deformation accompanied by an internal structural reorganization.[36] During this process, half of the oxygen atoms are displaced from their initial positions, breaking a quarter of the Sm−O bonds and forming new bonds such that the atomic arrangement of zircon is transformed into the atomic arrangement of scheelite. This bond-switching process does not result in changes in bond lengths but induces alterations inside the SmO_8 bisdisphenoids, which are the central point of the zircon−scheelite transformation.

Before concluding this work, we would like to comment that color changes were observed in the samples after the phase transitions. These facts suggest that monazite $PrVO_4$ and scheelite $SmVO_4$ have a smaller optical band gap (E_{gap}) than their zircon phases which have E_{gap} = 3.7−3.8 eV.[37] This observation is consistent with the band gap collapses observed at the zircon−monazite transition in $NdVO_4$[37] and at the zircon−scheelite transition in $YbVO_4$.[37] These collapses range from 0.5 to 1 eV. Our conclusions are also in agreement with predictions that can be extracted from band-structure calculations.[1,37−39] This suggests that the metastable HP polymorphs can find novel applications for rare-earth vanadates. One interesting possibility to explore in the future is their use as photocatalysts for H_2 evolution and sunlight-driven photodegradation,[40] which can be a significant contribution to the field of renewable energy sources.

4. CONCLUDING REMARKS

We presented room-temperature Raman measurements in $PrVO_4$ and $SmVO_4$ up to 17 GPa. In the first compound we detect an irreversible phase transition from zircon to monazite at 6 GPa. In the second compound an irreversible phase transition from zircon to scheelite is found at 6.5 GPa. The crystal structure of the HP phases was determined by XRD measurements of samples synthesized at 12 GPa using a large-volume press. The pressure evolution of the Raman modes of different polymorphs is also presented and discussed. The reported results contribute to better a understanding of the HP structural and lattice-dynamics properties of orthovanadates. The isolation of the metastable HP phases of $PrVO_4$ and $SmvO_4$ could have great importance for chemists and the technological applications of these compounds.

AUTHOR INFORMATION

Corresponding Author

*E-mail: daniel.errandonea@uv.es.

Author Contributions

The manuscript was written through contributions of all authors. All authors have given approval to the final version of the manuscript.

Notes

The authors declare no competing financial interests.

ACKNOWLEDGMENTS

Research was supported by the Spanish government MINECO under grant nos. MAT2010-21270-C04-01 and CSD2007-00045. S.N. Achary acknowledges the support provided by Universitat de Valencia during his visit to it.

REFERENCES

(1) Huang, Z.; Zhang, L.; Pan, W. *Inorg. Chem.* **2012**, *51*, 11235−11237 and references therein.

(2) Aldred, T. *Acta Crystallogr., Sect. B: Struct. Sci.* **1984**, *40*, 569−574 and references therein.

(3) Errandonea, D.; Lacomba-Perales, R.; Ruiz-Fuertes, J.; Segura, A.; Achary, S. N.; Tyagi, A. K. *Phys. Rev. B* **2009**, *79*, 184104.

(4) Errandonea, D.; Kumar, R. S.; Achary, S. N.; Tyagi, A. K. *Phys. Rev. B* **2012**, *84*, 224121.

(5) Mittal, R.; Garg, A. B.; Vijayakumar, V.; Achary, S. N.; Tyagi, A. K.; Godwal, B. K.; Busetto, E.; Lausi, A.; Chaplot, S. L. *J. Phys.: Condens. Matter* **2008**, *20*, 075223.
(6) Lacomba-Perales, R.; Errandonea, D.; Meng, Y.; Bettinelli, M. *Phys. Rev. B* **2010**, *81*, 064113.
(7) Zhang, F.; Wang, J. W; Lang, M.; Zhang, J. M.; Ewing, R. C. *Phys. Rev. B* **2009**, *80*, 184114.
(8) Errandonea, D.; Kumar, R. S.; Lopez-Solano, J.; Rodrıguez-Hernandez, P.; Muñoz, A.; Rabie, M. G.; Saez Puche, R. *Phys. Rev. B* **2011**, *83*, 134109.
(9) Stavrou, E.; Tatsi, A.; Raptis, C.; Efthimiopoulos, I.; Syassen, K.; Muñoz, A.; Rodrıguez-Hernandez, P.; Lopez-Solano, J.; Hanfland, M. *Phys. Rev. B* **2012**, *85*, 024117.
(10) Klotz, S.; Paumier, L.; Le Marchand, G.; Munsch, P. *J. Phys. D: Appl. Phys* **2009**, *42*, 075413.
(11) Mao, H. K.; Xu, J.; Bell, P. M. *J. Geophys. Res.* **1986**, *91*, 4673–4676.
(12) Chakoumakos, B. C.; Abraham, M. M.; Boatner, L. A. *J. Solid State Chem.* **1994**, *109*, 197–202.
(13) Mullica, D. F.; Sappenfield, E. L.; Abraham, M. M.; Chakoumakos, B. C.; Boatner, L. A. *Inorg. Chim. Acta* **1996**, *248*, 85–88.
(14) Errandonea, D. *J. Appl. Phys.* **2010**, *108*, 033517.
(15) Errandonea, D.; Martínez-García, D.; Segura, A.; Ruiz-Fuertes, J.; Lacomba-Perales, R.; Fages, V.; Chevy, A.; Roa, L.; Muñoz-San José, V. *High Pressure Res.* **2006**, *26*, 513–518.
(16) Santos, C. C.; Silva, E. N.; Ayala, A. P.; Guedes, I.; Pizani, P. S.; Loong, C. K.; Boatner, L. A. *J. Appl. Phys.* **2007**, *101*, 052511.
(17) Guedes, I.; Hirano, Y.; Grimsditch, M.; Wakabayashi, N.; Loong, C. K.; Boatner, L. A. *J. Appl. Phys.* **2001**, *90*, 1843–1846.
(18) Panchal, V.; Manjón, F. J.; Errandonea, D.; Rodríguez Hernández, P.; López-Solano, J.; Muñoz, A.; Achary, S. N.; Tyagi, A. K. *Phys. Rev. B* **2011**, *83*, 064111.
(19) Rao, R.; Garg, A. B.; Sakuntala, T.; Achary, S. N.; Tyagi, A. K. *J. Solid. State Chem.* **2009**, *182*, 1879–1883.
(20) Panchal, V.; Lopez-Moreno, S.; Santamarıa-Perez, D.; Errandonea, D.; Manjon, F. J.; Rodrıguez-Hernandez, P.; Muñoz, A.; Achary, S. N.; Tyagi, A. K. *Phys. Rev. B* **2011**, *84*, 024111.
(21) Garg, A. B.; Rao, R.; Sakuntala, T.; Wani, B. N.; Vijayakumar, V. *J. Appl. Phys.* **2009**, *106*, 063513.
(22) Duclos, S. J.; Jayaraman, A.; Espinosa, G. P.; Cooper, A. S.; Maines, R. G. *J. Phys. Chem. Solids* **1989**, *50*, 769–775.
(23) Patel, N. N.; Garg, A. B.; Meenakshi, S.; Pandey, K. K.; Wani, B. N.; Sharma, S. M. *AIP Conf. Proc.* **2010**, *1313*, 281–283.
(24) Zhang, C. C.; Zhang, Z. M.; Dai, R. C.; Wang, Z. P.; Zhang, J. W.; Ding, Z. J. *J. Phys. Chem. C* **2010**, *114*, 18279–18282.
(25) Stavrou, E.; Tatsi, A.; Salpea, E.; Boulmetis, Y. C.; Kontos, A. G.; Raptis, Y. S.; Raptis, C. *J. Phys.: Conf. Ser.* **2008**, *121*, 042016.
(26) Silva, E. N.; Ayala, A. P.; Guedes, I.; Paschoal, C. W. A.; Moreira, R. L.; Loong, C. K.; Boatner, L. A. *Opt. Mater.* **2006**, *29*, 224–230.
(27) Bandiello, E.; Errandonea, D.; Martinez-Garcia, D.; Santamaria-Perez, D.; Manjon, F. J. *Phys. Rev. B* **2012**, *85*, 024108.
(28) Porto, S. P. S; Scott, J. F. *Phys. Rev.* **1967**, *157*, 716–719.
(29) Manjón, F. J.; Errandonea, D.; Garro, N.; Pellicer-Porres, J.; Rodríguez-Hernández, P.; Radescu, S.; López-Solano, J.; Mujica, A.; Muñoz, A. *Phys. Rev. B* **2006**, *74*, 144111.
(30) Frost, R. L. *J. Raman Spectrosc.* **2004**, *35*, 153–158.
(31) Gomis, O.; Sanz, J. A.; Lacomba-Perales, R. L.; Errandonea, D.; Meng, Y.; Chervin, J. C.; Polian, A. *Phys. Rev. B* **2012**, *86*, 054121.
(32) Rice, C. E.; Robinson, W. R. *Acta Crystallogr., Sect. B: Struct. Crystallogr. Cryst. Chem.* **1976**, *32*, 2232–2233.
(33) Range, K. J.; Meister, H. *Acta Crystallogr., Sect. C: Cryst. Struct. Commun.* **1990**, *46*, 1093–1094.
(34) Clavier, N.; Podor, R.; Dacheux, N. *J. Europ.Ceram. Soc.* **2011**, *31*, 941–976.
(35) Florez, M.; Contreras-Garcia, J.; Recio, J. M.; Marques, M. *Phys. Rev. B* **2009**, *79*, 104101.
(36) Smirnov, M. B.; Mirgorodsky, A. P.; Kazimirov, V. Y.; Guinebretière, R. *Phys. Rev. B* **2008**, *79*, 094109.
(37) Panchal, V.; Errandonea, D.; Segura, A.; Rodrıguez-Hernandez, P.; Muñoz, A.; Lopez-Moreno, S.; Bettinelli, M. *J. Appl. Phys.* **2011**, *110*, 043723.
(38) Sun, L.; Zhao, X.; Li, Y.; Li, P.; Sun, H.; Cheng, X.; Fan, W. *J. Appl. Phys.* **2010**, *108*, 093519.
(39) Dolgos, M. R.; Paraskos, A. M.; Stoltzfus, M. W.; Yarnell, S. C.; Woodward, P. M. *J. Solid State Chem.* **2009**, *182*, 1964–1971.
(40) Nagabhushana, G. P.; Nagaraju, G.; Chandrappa, G. P. *J. Mater. Chem. A* **2013**, *1*, 388–394.